Energy calibration of the JLab bremsstrahlung tagging system

S. Stepanyan[a,*], S. Boyarinov[a], H. Egiyan[a,b], L. Guo[a], D. Dale[c], M. Gabrielyan[c], L. Gan[f], A. Gasparian[g], A. Glamazdin[d], B. Mecking[a], I. Nakagawa[c,1], A. Teymurazyan[c], M.H. Wood[e]

[a]Thomas Jefferson National Accelerator Facility, Newport News, VA 23606, USA
[b]Department of Physics, University of New Hampshire, Durham, NH 03824, USA
[c]Department of Physics and Astronomy, University of Kentucky, Lexington, KY 40506, USA
[d]Kharkov Institute of Physics and Technology, Kharkov 61108, Ukraine
[e]Department of Physics, University of Massachusetts, Amherst, MA 01003, USA
[f]University of North Carolina at Wilmington, S. College Rd., Wilmington, NC 28403, USA
[g]North Carolina A&T State University, Greensboro, NC 27411, USA

Abstract

In this report, we present the energy calibration of the Hall B bremsstrahlung tagging system at the Thomas Jefferson National Accelerator Facility. The calibration was performed using a magnetic pair spectrometer. The tagged photon energy spectrum was measured in coincidence with e^+e^- pairs as a function of the pair spectrometer magnetic field. Taking advantage of the internal linearity of the pair spectrometer, the energy of the tagging system was calibrated at the level of $\pm0.1\%E_\gamma$. The absolute energy scale was determined using the e^+e^- rate measurements close to the end-point of the photon spectrum. The energy variations across the full tagging range were found to be $<3\,\mathrm{MeV}$.
© 2007 Elsevier B.V. All rights reserved.

1. Introduction

In this report, we present the method and the results of the energy calibration of the Hall B photon tagging system [1] at the Thomas Jefferson National Accelerator Facility (JLab). The Hall B tagging system provides tagged photons in the multi-GeV energy range with high energy resolution ($\sim0.1\%E_\gamma$) and a broad tagging range, $20-95\%$ of E_0. It is used for the investigation of real photon induced reactions, primarily in conjunction with the CEBAF Large Acceptance Spectrometer (CLAS) [2]. The tagging range of the device is divided into 767 energy bins (E-bins). In each E-bin, the central value of the energy is used as the energy of the radiated photon. These values were generated by a ray-tracing program using the design geometry of the scintillation counter hodoscope (384 overlapping counters, called E-counters) and the two-dimensional field map of the dipole magnet.

In the analysis of fully exclusive reactions, such as photoproduction on deuterium,[2] it was found that the photon energy defined by CLAS and the central values of the E-bins of tagged photons are different by as much as 0.5%. The variation of this difference as a function of the tagger E-counter position was compatible with a possible sag of the frames which hold the E-counters. There was corroborating evidence from simulations of the effects of gravitational sagging and various possible misalignments of the tagger focal plane [4].

---

*Corresponding author. Tel.: +1 757 269 7196; fax: +1 757 269 5800.
  E-mail address: stepanyan@jlab.org (S. Stepanyan).
[1]Current address: The Institute of Physical and Chemical Research (RIKEN), Wako, Saitama 351-0198, Japan.

---

[2]In the kinematically complete reaction $\gamma d \rightarrow p\pi^+\pi^-(n)$ the neutron mass was used as a constraint to calculate the photon energy from the momenta of the charged particles [3].

To determine corrections to the central value of energy in each E-bin independent of CLAS, the tagged photon energy spectrum was measured in coincidence with e^+e^- pairs detected in the Hall-B pair spectrometer (PS) [5]. The data were collected as a function of the PS dipole field and at fixed geometry of the e^+e^- detectors. These measurements, taking advantage of the linear relationship between momentum and the magnetic field of the PS, allowed for the relative calibration of E-bins with high accuracy. Using measurements of e^+e^- coincidence rates at PS settings close to the end-point energy, the absolute energy scale of the tagging system was calibrated as well. The energy correction factor for each E-bin is defined as the ratio of photon energy, determined from momenta of e^+e^- pairs, to the ideal central value of the energy of that E-bin.

To calculate the momenta of the e^+ and e^-, a simplified model for a homogeneous dipole was employed, using central value of the field and the positions of the particle trajectories at the entrance and exit of the field region. Two corrections were introduced to the model based on ray-tracing simulations using measured and generated field maps to account for non-linearities in the field distribution and for the finite beam and detector sizes.

For these measurements, the PS was instrumented with micro-strip detectors for better position determination of e^+ and e^-, and thus better energy resolution. Based on the level of knowledge of the PS dipole field distribution and the position of the micro-strip detectors, the accuracy of the method is estimated to be $\delta E_\gamma \sim \pm 0.1\% E_\gamma$.

2. Experimental setup and the measurements

The data were collected during a photoproduction experiment in April of 2004 using the Hall B bremsstrahlung tagging system and the PS. The description of the tagging system can be found in Ref. [1], a schematic view of the setup is shown in Fig. 1. The photon beam was generated in the interaction of a $E_e = 3.776$ GeV electron beam with a 10^{-4} radiation length thick Au foil ("Radiator"). The tagger dipole magnet was operated at 1273 A current (corresponding to the central field value of 1.0627 T) and covered the tagged photon energy range from 0.9 to 3.6 GeV. The Hall B PS is located ~10 m downstream of the "Radiator." The PS consists of a dipole magnet and two planes of scintillation counters, positioned symmetrically to the left and the right of the beam axis in the horizontal plane downstream of the magnet. The pair production converter, "Pair converter", is located 55.8 cm upstream of the PS dipole center and consists of 10^{-3} radiation length thick Aluminum.

For this measurement, in addition to the scintillation detectors, the PS was instrumented with two pairs of micro-strip detectors (MS) to provide better position determination for the e^+e^- behind the dipole. They were mounted 93.07 cm downstream of the magnet center, in front of the scintillation counters. Each pair of micro-strip detectors consisted of X and Y planes and covered 20×20 mm^2 of detection acceptance. (The (XZ) plane is defined by the centerline of the beam and the deflection plane of the dipole. The main field component is parallel to the Y-axis.) The distance between the centroids of the "X" planes was 450 ± 0.5 mm, and they were centered on the beam axis. The pitch size of the micro-strip detectors was 50 μm. In the off-line analysis, only one of the "Y" planes was used, since the micro-strip for the second "Y" plane had a high noise level.

The measurements were conducted at a large number of settings of the PS dipole field in the range from 0.36 to 1.3 T which corresponds to PS currents from 543 to 2278 A. At this range of the field values, the energy range of e^+e^- covered almost the full energy range of the tagging system, see Fig. 2. The PS magnetic field value was measured with a Hall probe positioned at the center of the magnet. The accuracy of the device in the range of the measured fields is
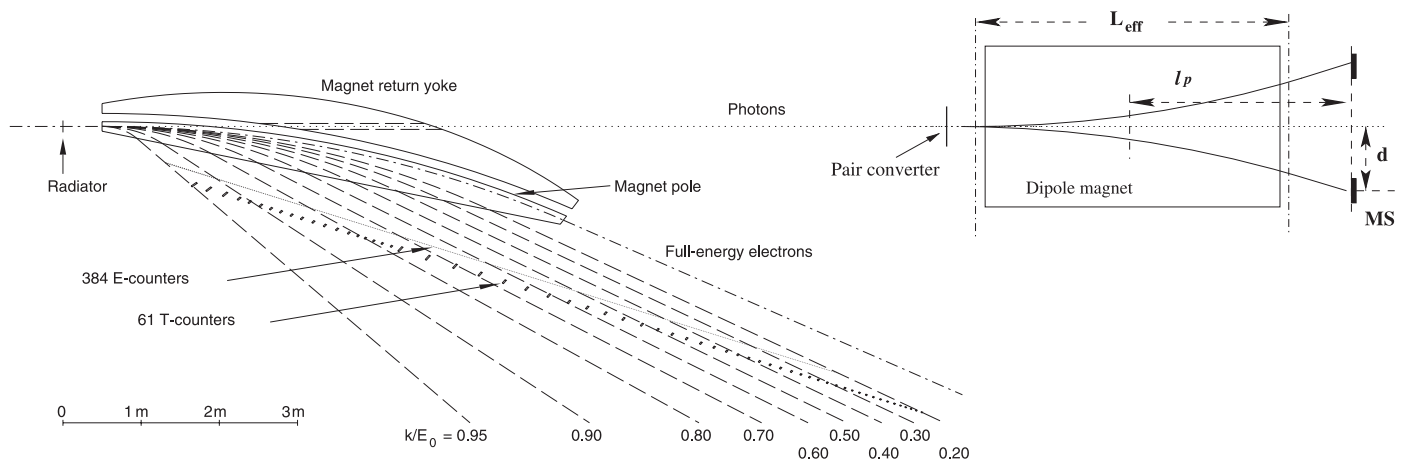

Fig. 1. Schematic view of the setup. The focal plane hodoscope consists of two planes of scintillation counters. The first plane, called E-plane, contains 384 overlapping counters, E-counters, and defines the energy bins. The second plane, called T-plane, contains 61 counters, T-counters, used for the time coincidence with CLAS. The pair production converter of the PS is located about 8 m downstream of the radiator. For illustration purposes the diagram of the PS is rotated by 90° around the beam axis.
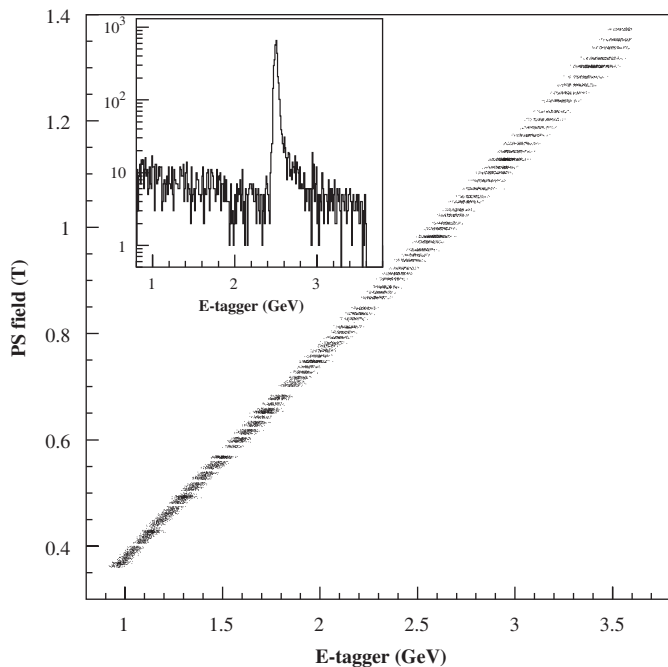
Fig. 2. Scatter plot of tagged photon energy values for each PS dipole magnetic field setting. The inset shows the tagged photon energy distribution at the PS dipole field of 0.97 T.

better than 10^{-3}. The entire data taking process was automated. At each field setting, data were acquired for 15 min of real beam time with a beam current > 5 nA. A total of 180 points at different field values were measured.

For the determination of the absolute energy scale, data were taken at PS field values from 1.35 to 1.9 T, corresponding to currents from 2073 to 2775 A, without requiring a coincidence with the tagging system. At these field values, the sum of energies of the detected e^+ and e^- covered the range slightly below and above the electron beam energy (the end-point of the bremsstrahlung spectrum). Measurements of the e^+e^- coincidence rate at a fixed acceptance of the detectors allowed us to relate the PS field values to the electron beam energy. Using this relation, the absolute energy scale in the pair spectrometer was defined.

3. Data analysis

A coincidence signal from the scintillator counters of the PS was used to form a trigger for the DAQ system. For each trigger, time information from the tagger E- and T-counters and the amplitude of the signals in each channel of the micro-strip detectors were recorded. Information on beam current, beam position, and magnetic field settings was inserted into the data stream every 10 s during data taking.

In the off-line analysis, events with tagger hits within 15 ns relative to the trigger were used. Hits in the tagger are selected using a tight timing coincidence between E-counters and the corresponding T-counter. The inset in Fig. 2 shows the tagged photon energy distribution at a

single setting of the PS dipole field (0.97 T) for selected tagger hits. The accidental background in the tagger was of the order of 1%.

For the determination of the intersection point of e^+e^- trajectories with the plane of micro-strip detectors, only channels with ADC values that were above the pedestal by more than five standard deviations were selected. Valid hits in both "X" planes and in one "Y" plane were required. The distributions of the number of hits in these planes are shown in Fig. 3. A small fraction of events with more than three hits in $X1$, $Y1$, or $X2$ planes was rejected. For the final analysis, events with two or three hits in a given plane were accepted if two of these hits were adjacent (the requirement of adjacent hits rejected only few events). In the bottom panel of Fig. 3, the number of adjacent hits vs. the number of hits on the $X1$ plane is plotted. The distributions in the $Y1$ and the $X2$ planes were similar. The hatched boxes on the graph correspond to the criteria for the event selection. For adjacent hits, the position on the plane is calculated as a weighted average using the ADC values.

To reduce uncertainties due to the PS angular acceptance, the e^+e^- scattering plane was limited to ± 0.25 cm around the detector mid-plane.

4. Tagger energy corrections

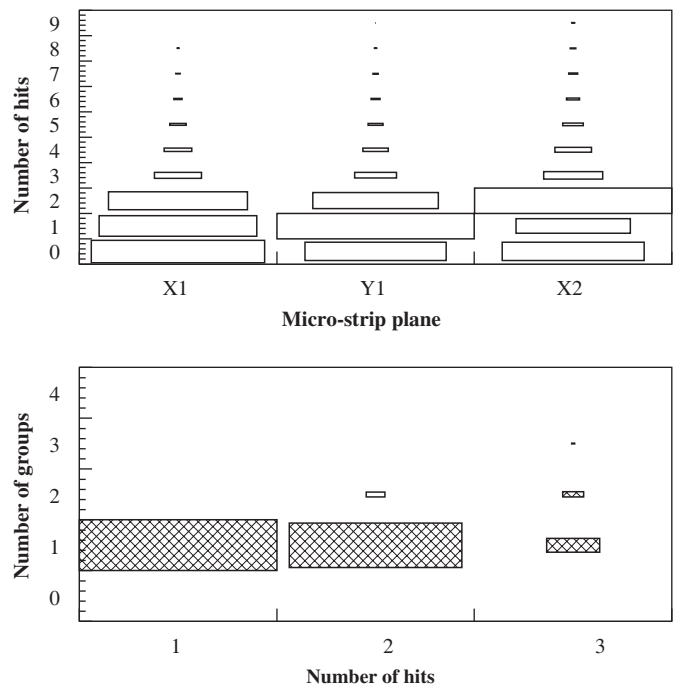The derivation of corrections to the tagger energy is performed in two steps. First, the mean values of the ratio

Fig. 3. Top panel: the distribution of the number of hits for the $X1$, $Y1$, and $X2$ planes of the micro-strip detector. Bottom panel: the distribution of the number of adjacent hits ("groups") as a function of the number of hits for 1, 2, and 3 hits cases of $X1$ plane. Shaded boxes are the combinations that were allowed for the analysis. The size of the boxes corresponds to the number of events.

of the photon energy, measured in the PS, to the central value of the E-bins were calculated. Then, these mean values were scaled by the ratio of the electron beam energy to the end-point energy measured in the PS.

The photon energy is defined as a sum of the e^+e^- energies reconstructed in the PS. The energies of the electron and the positron were reconstructed in a simplified model for charged particle propagation through the magnetic field. The ratios were calculated on an event-by-event basis for each E-bin that was within the acceptance range of the PS at a given field setting.

The scale factor for the absolute energy determination in PS was derived from studies of the e^+e^- coincidence rate as a function of the energy reconstructed in PS.

4.1. Model for photon energy reconstruction in PS

In Fig. 1, the particle trajectories passing through the magnetic field of the PS dipole magnet are shown by the solid-lines. For each event, the transverse displacements of the trajectories from the beam centerline (d) for the e^+ and the e^- were measured in the micro-strip detector plane. The momenta of leptons (P) were calculated in a model that assumes a uniform field distribution between the two points along the trajectory of the particle. In this approximation the momentum can be expressed as a linear function of the magnetic field strength, B, and the radius of curvature, R

$$P = 0.2997925 \cdot R \cdot B_0 \qquad (1)$$

where P is in GeV/c, B in T, and R in m. The radius of curvature is defined as

$$R = L_{\text{eff}} \cdot \sqrt{\left(\frac{l_p}{d_e}\right)^2 + 1} \qquad (2)$$

where L_{eff} is the effective field length, l_p is the distance from the magnet center to the detector plane, and d_e is the transverse displacement of the trajectory at the detector plane.

The effective field length is defined as

$$L_{\text{eff}} = \frac{\int B \, \mathrm{d}l}{B_0} \qquad (3)$$

where the integral is measured along the trajectory and B_0 is the field value in the center of the magnet. The ratio was calculated using the simulation of trajectories by the Runge–Kutta–Nystroem method and the field map generated using a TOSCA [6] model for the magnet. The generated field map was used in the simulation due to the limited number of measured points for the magnetic field in the acceptance region of the setup. Fig. 4 shows the dependence of L_{eff} on the magnetic field for the central trajectory inside the acceptance region of the detector. The drop of L_{eff} at high B_0 is due to saturation effects. It was parametrized using a third order polynomial function for the range of field values > 0.8 T and a linear function for
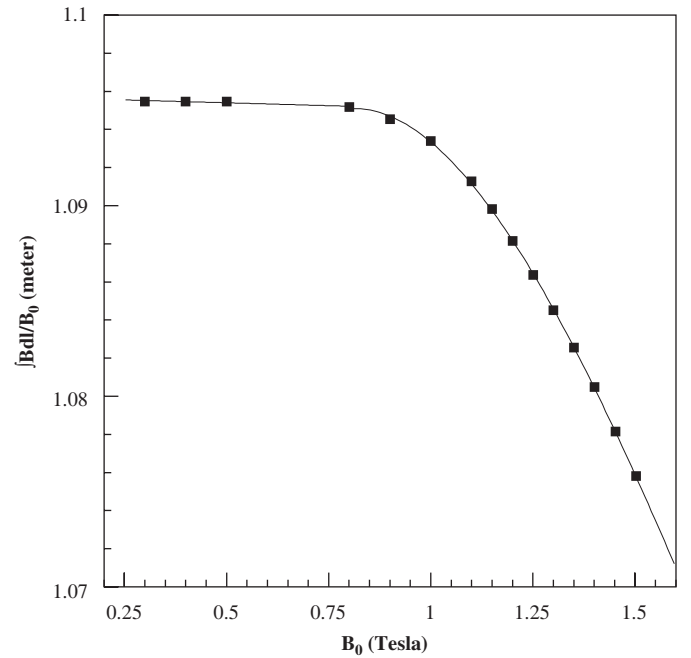

Fig. 4. Dependence of L_{eff} on B_0, data points. The solid line is the fitted function used in the analysis.

the range < 0.8 T. The parametrization was then used to calculate the particle momentum. The effects of the finite detector sizes, detector geometry, and the size of the beam on L_{eff} were convoluted into a correction function, $G(d_{e^+}, d_{e^-})$, as explained below. For data analysis, another correction function, $F(B_0)$, was introduced to account for the difference between the generated and the real field distributions.

The photon energy, E_γ^c, was defined as a sum of the e^+ and the e^- energies with correction factors $G(d_{e^+}, d_{e^-})$ and $F(B_0)$.

$$E_\gamma = (E_{e^+} + E_{e^-}) \cdot G(d_{e^+}, d_{e^-}) \cdot F(B_0). \qquad (4)$$

As shown below, using the simulated field, the accuracy of the approximation of Eq. (4) is better than the required accuracy for these measurements ($< 10^{-3}$).

4.2. Correction for the detector geometry

In order to determine the function $G(d_{e^+}, d_{e^-})$, pairs of opposite sign trajectories, originating from the same point at the pair converter T, were generated for several PS field values in a large momentum space. The simulations covered the full energy range of measurements. The starting points of the trajectories were distributed in the transverse direction according to the photon beam profile, using a Gaussian with $\sigma \simeq 1$ mm. As a correction function $G(d_{e^+}, d_{e^-})$, the ratio of the sum of generated momenta to the sum of reconstructed momenta using Eq. (1) was defined. In Fig. 5 the dependence of this ratio on the distance between e^+ and e^- for the central field value $B_0 = 0.3$ T is presented. An almost linear dependence was observed with very small variations ($< 0.3\%$) over a large

range of distances. The negative slope of the dependence reflects the fact that L_{eff} was calculated for the central trajectory that corresponds to $d_{e^+} + d_{e^-} = 45$ cm. For tracks with $d_{e^+} + d_{e^-} < 45$ cm ($d_{e^+} + d_{e^-} > 45$ cm), $\int B\,dl$, and therefore the effective field length, is smaller (bigger) than for the central trajectory. The overall scale of the ratio, <1, is due to an asymmetric distribution of the field between tracks start and end points, the MS plane is located farther from the magnet center than the pair converter. It should be noted that in the detector geometry of the experiment, $d_{e^+} + d_{e^-}$ spans the range from 43 to 47 cm. A third-degree polynomial function was used to fit the dependence in Fig. 5.

Similar dependences were obtained for several other field settings. In Fig. 6, the distribution of the ratio for several field values (up to 1.5 T), divided by the dependence obtained at 0.3 T, is presented. The distribution is centered at unity with an RMS value of 1.6×10^{-4}, indicating that the function $G(d_{e^+} + d_{e^-})$ found at 0.3 T describes the position dependence at all fields very well.

4.3. Correction for using a simulated field

The effective field length was calculated based on the TOSCA-generated field map [6]. In Fig. 7, a comparison of the generated (dots) and the measured (open squares) field distributions is presented. There is a small difference in the fringe field and, therefore, another correction factor was introduced to account for this difference. To derive this correction factor, the $\int B\,dl$ values along the Z-axis for the measured and the TOSCA-calculated field distributions were studied. Since the number of points where the B-field

Fig. 6. Distribution of the ratio of generated and reconstructed momenta for several central field values, R, normalized to the ratio at $B_0 = 0.3$ T, $R(0.3)$, for 15 points in $(d_1 + d_2)$ at each field setting.
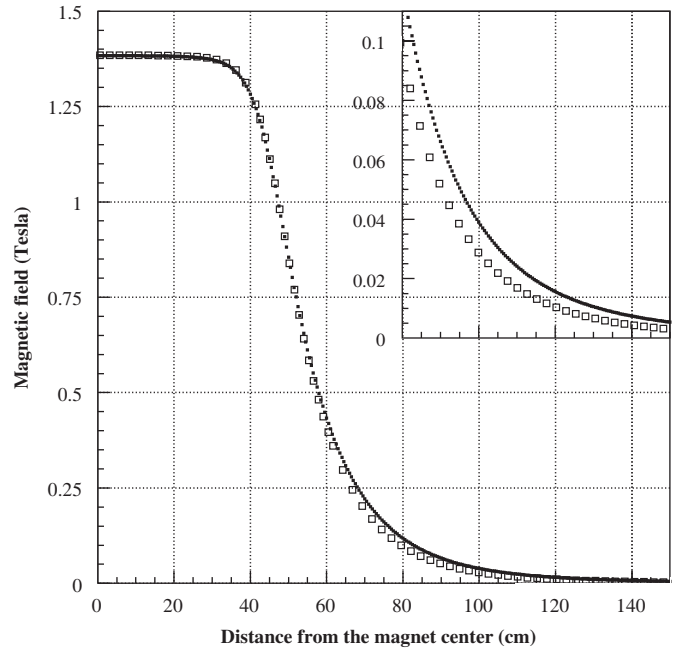
Fig. 7. Comparison of the measured and TOSCA-calculated fields.

was measured was too small to define the integral along the real trajectories, we compared integrals along the Z-axis. The ratio of these integrals was studied for four different transverse positions, $X = 0, 8.5, 13.6, 18.7$ cm. In Fig. 8a, the dependence of the ratio on the magnetic field value is shown. For the $X = 0$ point, the Z-dependence of the field was measured at eight settings and, therefore, the ratio was defined for eight field settings. At $X = 8.5, 13.6, 18.7$ cm,
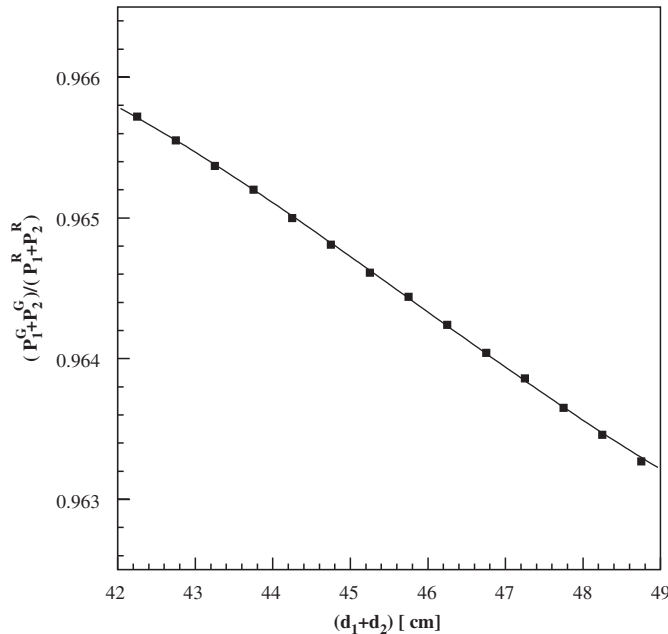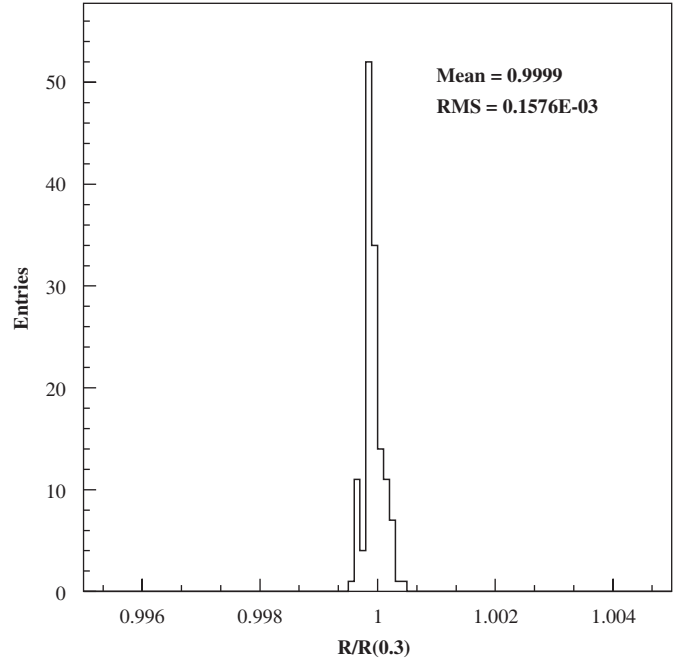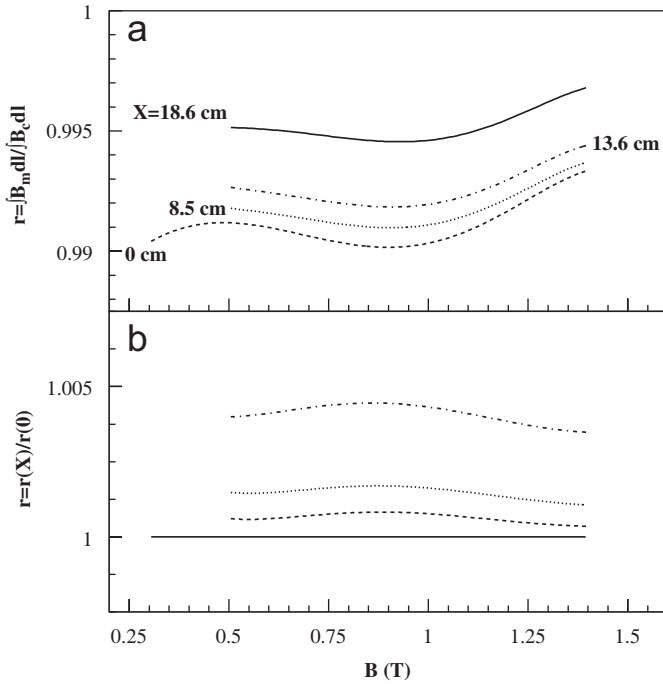

Fig. 5. Dependence of the ratio of the total momenta of the simulated pair to the sum of the reconstructed momenta, as defined in Eq. (1), on $(d_1 + d_2)$. The central field value was $B_0 = 0.3$ T.

Fig. 8. Comparison of $\int B\,\mathrm{d}l$ values along the Z axis, calculated using the measured and the TOSCA-calculated field distributions. (a) the ratio of integrals at different distances from the magnet centerline: the dashed line at $X = 0$, the dotted line at $X = 8.5\,\mathrm{cm}$, the dashed-dotted line at $X = 13.6\,\mathrm{cm}$, and the solid line at $X = 18.6\,\mathrm{cm}$. In (b) the same ratios normalized to the ratio at $X = 0$.

Fig. 9. Fit to the $E_\gamma / E_{\mathrm{tag}}^i$ distributions for E-counters #76, 149, 391, and 576. As a fit function a sum of two Gaussian and a linear function is used. The mean of the narrow Gaussian, that describes the main peak, was used to determine the correction factor to the tagger energy, C_i.

measurements are available for only five settings of the PS field. The absolute scale of the ratio depends on X, but the shape is similar for all X values. Since the real trajectories cover a larger range of X, and the absolute energy scale will be defined by the end-point measurements (see below), the absolute scale of the ratio is not important. For the analysis, the shape of the fitted dependence, $F(B)$, at $X = 0$ was used. The uncertainty in the determination of the $F(B)$ is one of the largest contributions to the uncertainty in the final corrections. As shown in Fig. 8(b), the estimated uncertainty of $F(B)$, based on the variations of $r(X)/r(0)$ for single X, is $\pm 0.05\%$.

4.4. Determination of the energy ratios

The distributions of the ratio $E_\gamma / E_{\mathrm{tag}}^i$ are shown in Fig. 9 for E-bins $i = 76$, 149, 391, and 576. Similar distributions have been analyzed for all E-bins. The distributions are fitted to a sum of two Gaussians and a linear function. In the figure, fit results are shown with lines. The mean value, C_i, of the narrow Gaussian, that describes the main peak, was used to determine the correction factor to the tagger energy.

5. End-point measurements

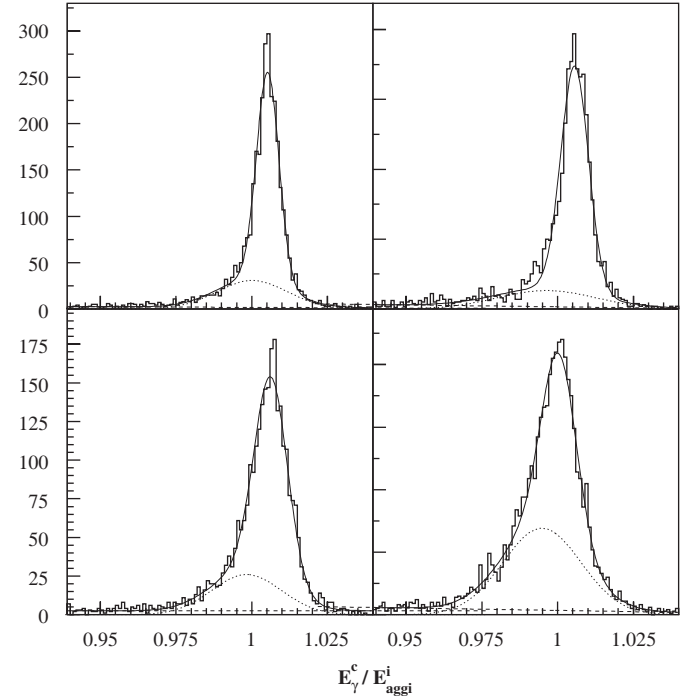For a given detector acceptance, an increase of the magnetic field value selects e^+e^- pairs from higher energy photons, and at some point reaches the end-point energy, E_0. Measurements of the e^+e^- coincidence rate as a function of the field value at fixed geometry allow to determine the relation between field value and the end-point energy of the photon beam. For these measurements the maximum energy of photons, or the energy of the electron beam, was $E_0 = 3.776\,\mathrm{GeV}$. This value was determined based on independent energy measurements performed in Hall A and in the accelerator. The difference between these two measurements was $\sim 3 \times 10^{-4}$ and was taken as the accuracy of the electron beam energy determination.

The e^+e^- coincidence rate was studied for several different detector geometries (different regions of X planes). In Fig. 10, the e^+e^- coincidence rate is plotted as a function of the photon energy, as defined in Eq. (4). Data obtained at the PS dipole field values from 1.35 to 1.9 T were combined. The shape of the end-point falloff is defined by the detector resolution. Radiative effects do not play a significant role at these energies [7]. The deviations from the lowest order bremsstrahlung cross-section at photon energies $\sim 0.999 E_0$ is estimated to be $< 10\%$. The energy value corresponding to the mid point of the falling edge, $E_{\mathrm{B}} = 3.784\,\mathrm{GeV}$, was taken as the end-point energy. The accuracy of this approximation was estimated to be of the order of 5×10^{-4}, using the results from studies with different detector acceptances and taking into account the 10% effect from radiative corrections. A scale factor $\eta = E_0/E_{\mathrm{B}} = 0.9985$ was found as a correction to the energy in
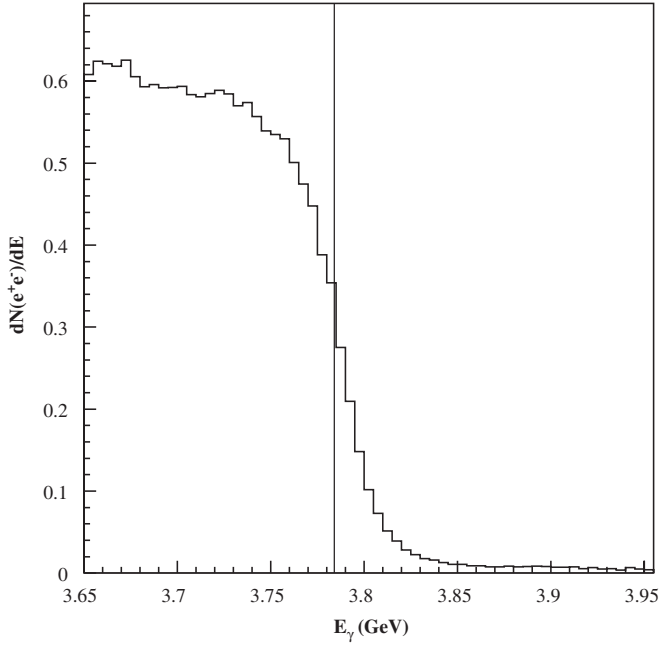
Fig. 10. The e^+e^- coincidence rate as a function of energy calculated using Eq. (4). The vertical line passes through the mid point of the falling edge, and is at $E = 3.784$ GeV.

Eq. (4), for the PS settings that were used to derive the correction factors C_i.

6. Final corrections

The final tagger energy corrections were computed using the C_i constants for each E-bin and the energy scale correction factor η. In Fig. 11, the final corrections are plotted as a function of the tagger energy bin. A few outlying points around the E-bins 120 and 440 are due to mis-cablings (which were found in this measurement and were fixed at a later time).

The estimated error in the determination of the C_i constants is 0.12%. It is defined by the accuracy of the approximation used in Eq. (1), 1.6×10^{-4}, by the determination of $F(B_0)$, 5×10^{-4}, by the error in the fit to the E_γ/E_{tag}^i distributions, $\sim 2 \times 10^{-4}$, and by the accuracy of the PS field measurement, $< 10^{-3}$. The fit error has a small energy dependence. It is small for high energy bins, 1.7×10^{-4}, and larger for the low energy bins, 3×10^{-4}. The error in the calculation of η arises from the determination of the end-point energy, 5×10^{-4}, and the knowledge of the electron beam energy, 3×10^{-4}. For the final correction constants the estimated total uncertainty is 0.13%.

In summary, we performed an energy calibration of the Hall B bremsstrahlung photon tagging system at Jefferson Lab. The calibration was done using the Hall B PS, instrumented with micro-strip detectors for high precision position measurements. The calibration results were checked using exclusive photoproduction reactions detected in CLAS. A result of such an analysis is presented in
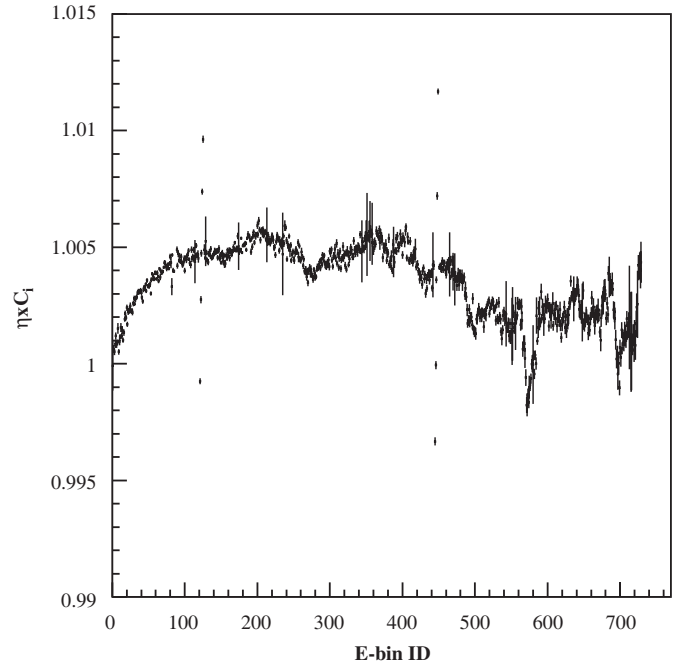

Fig. 11. The final tagger energy corrections for each E-bin. Smaller E-bin numbers correspond to higher photon energies.
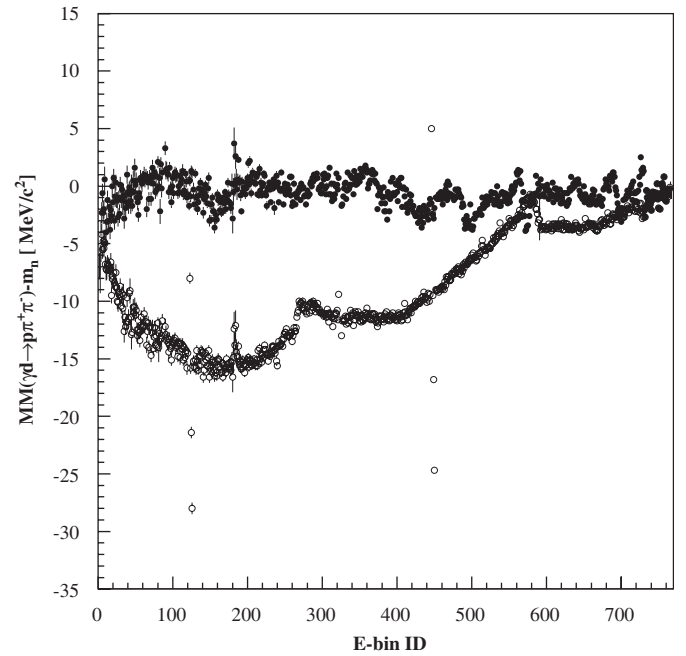

Fig. 12. The difference between the missing mass of the $(p\pi^+\pi^-)$ system in the reaction $\gamma d \rightarrow p\pi^+\pi^-(n)$ and the nominal neutron mass as a function of the tagger E-bin. Open symbols correspond to the missing mass calculation without and the filled symbols with the new tagger energy corrections.

Fig. 12. The exclusive reaction $\gamma d \rightarrow p\pi^+\pi^-(n)$ was studied where the final state proton and two pions were detected in CLAS, and the neutron was reconstructed from the missing momentum and missing energy analysis. In the figure, the difference of the missing mass of $(p\pi^+\pi^-)$ and the nominal mass of the neutron from the Particle Data Group (PDG)

[8] is plotted as a function of tagger E-bin. The open symbols correspond to the missing mass obtained without tagger energy corrections, and the filled symbols correspond to results when the tagger energy corrections were applied. The variation of the neutron missing mass without the corrections are up to 15 MeV, while with corrections these variations are within ± 3 MeV.

The analysis presented in Ref. [3] was repeated with the new calibration constants and showed similar improvements in the energy determination. The data in Ref. [3] were from a 1999 CLAS run, while the data used in this analysis and the data presented in Fig. 12 were taken in 2004. Comparison of these two sets of data shows that the geometry of the tagger focal plane did not change during this five year period and that the sagging and misalignments were introduced at the time of the tagger construction.

Acknowledgments

References

[1] D.I. Sober, et al., Nucl. Instr. and Meth. A 440 (2000) 263.
[2] B.A. Mecking, et al., Nucl. Instr. and Meth. A 503 (2003) 513.
[3] S. Stepanyan, CLAS-ANALYSIS 2003-105.
[4] D.I. Sober, H. Crannell, F.J. Klein, CLAS-NOTE 2004-019.
[5] The Hall B pair spectrometer was developed and constructed by the PrimEx collaboration at JLab ⟨http://www.jlab.org/primex/⟩.
[6] OPERA-3D User Guide, Vector Fields Limited, UK.
[7] H.D. Schultz, G. Lutz, Phys. Rev. 167 (1968) 1280.
[8] Particle Data Group, Phys. Lett. B 521 (2004).